Available online at www.sciencedirect.com
SCIENCE DIRECT®
Nuclear Instruments and Methods in Physics Research A 515 (2003) 829–839
NUCLEAR INSTRUMENTS & METHODS IN PHYSICS RESEARCH Section A
www.elsevier.com/locate/nima

A statistical correction method for minimization of systemic artefact in a continuous-rotate X-ray based industrial CT system

Umesh Kumar[a,*], G.S. Ramakrishna[a], A.S. Pendharkar[a], S. Kailas[b]

[a] *Isotope Applications Division, Bhabha Atomic Research Centre, Mumbai 400 085, India*
[b] *Nuclear Physics Division, Bhabha Atomic Research Centre, Mumbai 400 085, India*

Received 4 June 2003; accepted 4 July 2003

Abstract

The use of a linear detector array (LDA) in X-ray computed tomography (CT) imaging is well established. Generally the CT system using an LDA operates in a fan-beam configuration. In a non-medical tomography set-up, the X-ray source and detectors are stationary and the object is rotated for scanning. Equi-spaced angular projections over a complete 360° object rotation are required for CT image reconstruction using standard Convolution Back Projection (CBP) algorithm as applied to the fan-beam scanning geometry. If there is a lack of timing synchronization between the LDA data acquisition system and the rotary motion in a continuous-rotate system, the incremental angle for the acquired projections may not be known exactly. The error may cause artefacts and blurring in the CT image. The present paper describes a possible way of numerically tuning the acquired transmission data matrix for minimization of such artefacts. It is based on finding out statistically similar projections, which represent 0° and 360° angular views. The correction method has been developed to avoid modification in detector hardware and interface devices. The experimental CT system for industrial applications has been developed by making use of an independent scintillator-based linear detector array, commonly used for on-line radiography of low-density specimens. The proposed data pre-processing algorithm with some experimental results as well as limitations of the correction method is discussed.

PACS: 87.59.Fm; 87.59.Jq; 87.59.−e; 42.30.Wb; 07.85.−m

Keywords: Tomography; NDT; LDA; CT artefact

1. Introduction

In non-medical imaging applications, transmission gamma or X-rays based computed tomography is often regarded as a supplementary non-destructive testing (NDT) tool to conventional radiography. With the availability of low cost linear detector arrays and constant potential X-ray equipments, a tomographic imaging system can be developed in a cost effective manner for experimental purpose provided the associated problems are taken care of. The specific areas

*Corresponding author. Tel.: +91-22-2559-3275; fax: +91-22-2550-5151.
E-mail address: umeshk@apsara.barc.ernet.in (U. Kumar).

0168-9002/$ - see front matter © 2003 Elsevier B.V. All rights reserved.
doi:10.1016/j.nima.2003.07.019

which demand special attention in the development of an experimental tomographic imaging system are: (a) system alignment, (b) motion instability and (c) artefacts arising due to scattering and polychromatic nature of the Bremsstrahlung X-rays. When a tomography system is developed out of the available detector systems and mechanical manipulators as well as associated instrumentation, it is quite possible that a lack of synchronization among various sub-systems shows up in different artefacts in the reconstructed image. Crawford and Gulberg [1] derived an algorithm based on convolution back projection for a fan beam geometry that has an angular-dependent displacement in its centre of rotation. Waggener et al. [2] developed a hybrid reconstruction algorithm for X-ray computed tomography for fan-beam geometry with a modified parallel beam reconstruction formula. The paper also discussed correction for centre of rotation shift during back projection. Though there are different tomographic image reconstruction algorithms [3,4] (e.g., algebraic reconstruction technique), which do not require equiangular and equi-spaced data set, it is learnt that the quality achieved by convolution back projection (CBP) from 360° data sets in case of fan beam configuration is superior in terms of achievable spatial and contrast resolution. A definite advantage of algebraic reconstruction techniques (ART) lies in its versatility. It can be carried out for any scanning geometry and even for incomplete data problems. This does not say that the results of ART are satisfactory for such problems [5]. Detailed mathematical treatment on the tomographic image reconstruction from transmission projection data can be found in Refs. [5–7]. A discussion on the exact sampling conditions for standard fan beam scanning geometry to obtain a certain resolution is given in Ref. [8]. Parker [9] has discussed an optimal reconstruction algorithm based on a minimal data set. A natural extension of the Parker short scan approach was provided by Silver [10] to include redundant data in fan beam geometry. There is no concern of radiation exposure to the specimen in general NDT applications of tomography. If the total scanning time is not significantly long, one would hardly find any compulsion to use algorithms optimised for reduced scan times for NDT applications.

Uses of LDAs and similar devices for radiographic and tomographic imaging have been reported earlier [11,12]. A faster way of generating line integrals or projection data for CT image reconstruction is by using a point source of radiation that emanates a fan-shaped beam. This passes through the object plane and falls on an array of detectors. In industrial tomography, the X-ray source and detectors are generally stationary and the object is placed on a rotary platform. The relative motion is set to get the desired number of fan projections. When a rotate-only CT system operates in start–stop (steps) mode, there is definite information on the angular position for each projection since the rotary part is programmed in that way. This ensures that there is almost no error in the numerical value of the angular increment, which is passed to the reconstruction program. In case of a hard-wired continuous-rotate system also, it may be quite possible to get actual angular positions very precisely. In a situation like the one discussed in this paper, the LDA system receives only an initial trigger and an on-board clock mechanism directs one complete read-out of the frame-buffer. The rotary speed has to be programmed in such a way that it makes exactly a complete rotation (360°) by the time the LDA completes the last read-out of the detector array. The angular increment can be calculated based on the number of projections acquired and passed on to the reconstruction program.

The projection data for CT reconstruction of a single slice in case of parallel beam geometry is given by

$$P_\phi(t) = \ln\left[\frac{I_0(\phi)}{I_t(\phi)}\right] = \int_{(\phi,t)} f(x,y)\,\mathrm{d}s \tag{1}$$

t is related to x, y and ϕ as

$$t = x\cos\phi + y\sin\phi \tag{2}$$

where ϕ is the projection angle, t is the distance in the detector plane from the projected rotation axis and I_t and I_0 are detected beam intensities with and without object in its path. Computed tomography reconstructs the object function $f(x,y)$

from the set of projection measurements $P_\phi(t)$. The complete set of projection data $P_\phi(t)$ over N_P projections with N_S rays per projections forms the sinogram. The reader may refer the textbook by Kak and Slaney [6] for a detailed mathematical treatment on co-ordinate transformation equations and image reconstruction algorithms. The discrete representation of Eq. (1) in case of projections acquired using a linear detector array can be given as follows:

$$P_i(n.a) = \ln\left[\frac{I_0(n.a)}{I_i(n.a)}\right] \quad (3)$$

for $1 \leqslant i \leqslant N_P$ and $1 \leqslant n \leqslant N_S$

Here the index i represents the angular view number and a is the detector pitch of the linear detector array. The quantity $(n.a)$ represents the pixel location along the length of the detector array. Therefore, $I_0(n.a)$ and $I_i(n.a)$ represent the detector pixel output in absence and in presence of the object, respectively. Fig. 3 shows discrete $I_i(n.a)$ data in sinogram representation. As evident from the mathematics of CT image reconstruction based on filtered back projection technique, the $N_S \times N_P$ grid of projection data points should be equi-spaced. In addition, the rows corresponding to 0° and 360° angular positions should represent the same projection as also the angular increment between any two consecutive rows must be the same and equal to $2\pi/(N_P - 1)$ radian. Any deviation from these requirements will lead to artefacts in the reconstructed image. CT artefacts manifest themselves in somewhat different ways, since the CT image is numerically reconstructed from a series of measurements. Studies have shown that the angle of each view must be known to within a few hundredth of a degree, and the linear position of each sample within a given projection must be known to within a few tens of micrometres [13]. In some cases, the problem can be corrected or reduced in software; in others, it can be fixed only by re-engineering the offending sub-system.

In this paper, a numerical method is described for correcting the transmission data matrix, to minimize artefacts caused by the instability in synchronization of data acquisition system and the angular scanning sequence of the mechanical system. It is based on finding out statistically similar projections, which represent 0° and 360° angular views. The methodology of the experiment reported here, was devised to avoid modifications in the detector hardware and interface devices. It is interesting to note that the proposed correction method works fine as long as the projections are acquired for over a complete rotation of the object.

2. Experimental system

The experimental CT system consists of a 160 kV_P/10 mA constant potential X-ray generating system with specified focal spots of 1.5 mm × 1.5 mm (large focal spot) and 0.4 mm × 0.4 mm (small focal spot) and a 512-element linear detector array supplied by Detection Technology Inc., Finland. The details of the detector array [14] are given in Table 1. Fig. 1 gives a schematic block diagram of the set-up. A three-axis PC based stepper motor controlled mechanical manipulator was used for object manipulation and system alignment. The source-to-detector distance $(S_O + S_D)$ and source-to-object distance (S_O) were 1120 and 920 mm, respectively. In addition, only a portion of the full length of the linear array was

Table 1
LDA specifications

Type of the detector system	GOS scintillator-based linear diode array
Number of pixels	512
Image buffer size	Max. 512 × 1600
Pixel size	0.8 mm (H) × 0.6 mm (W)
Detector pitch	0.8 mm
Length of active area	410 mm
ADC resolution	12 bits
Control signal (PC to module)	Via RS 232 interface
Data transfer (module to PC)	Via RS 422 interface
Onboard offset and gain calibration	Yes
External trigger	Optical trigger sensor (reflecting type)
Make	Xscan08 of Detection Technology Inc., Finland

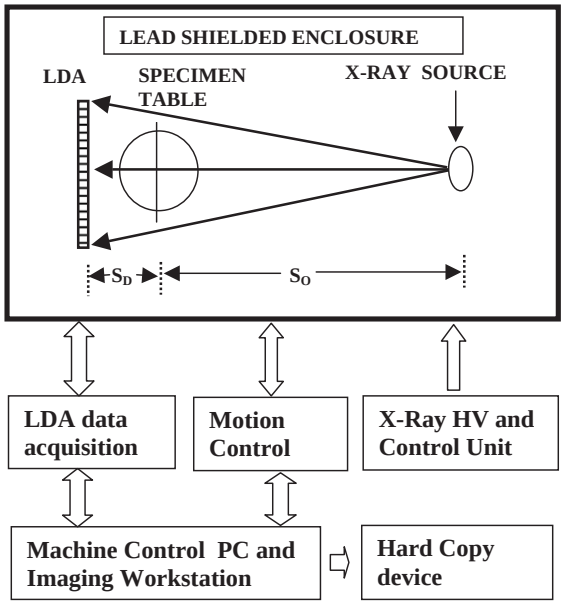

Fig. 1. Schematic block diagram of LDA tomography system.

Fig. 2. A partial photographic view of the experimental system.

used such that 260 detector elements symmetrically around the central ray fully covered the circle of reconstruction. The arrangement made use of a fan beam angle of approximately 10°. This was done so that the active detector pixels receive a relatively uniform X-ray flux. Fig. 2 shows a partial photographic view of the experimental set-up.

The mechanism of initiating trigger to the control unit of the linear detector array can be explained as follows. The object is mounted on the specimen platform, which is reset to zero position. The constant angular speed of the rotary axis is roughly calculated based on the read-out speed of the LDA data acquisition system. In this experiment, the LDA was programmed for a read-out speed of approximately 125 lines per second. It is obvious that the angular speed of the scanning mechanism should be set in such a way that it makes one complete revolution in the same time as the LDA takes to acquire a total of 1600 lines. As the corresponding angular positions for each transmission data set is not recorded on the fly, it is observed that the error in the calculated angular increment value causes artefact in the form of radially split images. This is probably because the calculated angular increment $\Delta\phi$ (rad) does not truly represent the angular separation between any two consecutive projections. $\Delta\phi$ is expressed in terms of N_P as

$$\Delta\phi = [2\pi/(N_P - 1)]. \quad (4)$$

This can be attributed to the fact that the last projection data ($N_P = 1600$) does not correspond to a projection at 2π radian angular location. As a result, reconstruction using filtered back projection method produces artefacts in the CT image. An earlier paper [15] provides a detailed description of the experimental system.

3. A statistical approach for correction

It can be observed that the projections of the same object distribution at 0° and 360° angular positions are the same provided there is no interference in the signal. This is, however, an ideal case as the signal will be corrupted by statistical and electronics noise. The correction method described here assumes that a full frame is acquired where the last line corresponds to an angular position slightly greater than 2π. Now as the frame represents over-sampled projection data, the next step is to find out index corresponding to the 2π angular positions. In order to have a uniform formulation so that the same can be implemented as part of the pre-processing sequence, the difference transmission data array is

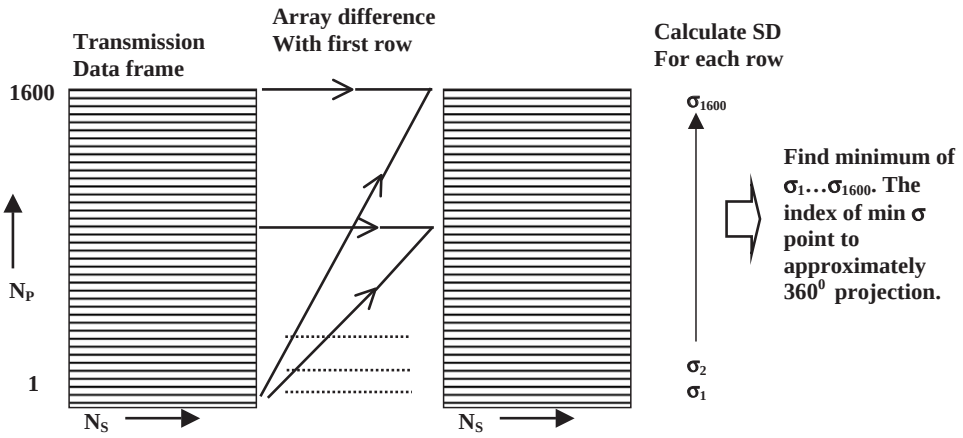

Fig. 3. Block diagram of the proposed numerical operations.

defined as

$$I_i^{\mathrm{Diff}}(t) = I_i(t) - I_{i=1}(t) \quad \text{for } 1 \leqslant i \leqslant N_{\mathrm{p}}. \tag{5}$$

The last $n_{\mathrm{p}}(\approx N_{\mathrm{P}}/4)$ projections are used to calculate the minimum of standard deviation (σ) in each row of the difference signal. The first minima relative to the top of the sinogram ($i = N_{\mathrm{P}}$) gives the index ($N_{\mathrm{P}}^{\#}$) corresponding to the 2π angular position data. The operation can be represented as

$$\sigma_{\min}[I_i^{\mathrm{Diff}}(t)] \Rightarrow N_{\mathrm{P}}^{\#}(i \equiv 2\pi) \tag{6}$$

where

$$\sigma\{I_i^{\mathrm{Diff}}(t)\} = \sqrt{\frac{\sum_{j=1}^{N_{\mathrm{S}}}\{I_i^{\mathrm{Diff}}(j) - \mathrm{mval}_i\}^2}{N_{\mathrm{S}}}}. \tag{7}$$

With

$$\mathrm{mval}_i = \frac{\sum_{j=1}^{N_{\mathrm{S}}}\{I_i^{\mathrm{Diff}}(j)\}}{N_{\mathrm{S}}}. \tag{8}$$

This leads to a value of $\Delta\phi$ as

$$\Delta\phi = 2\pi/(N_{\mathrm{P}}^{\#} - 1). \tag{9}$$

In order to have another parameter to verify, the minimum of mean squared error (mse) corresponding to each row of the difference signal was also calculated in the same way. The index ($i = N_{\mathrm{P}}^{\#}$) of the minimum of mse would be a pointer to the approximate 360° projection data. Mean squared error is defined as

$$\mathrm{mse}_i = \frac{\sum_{j=1}^{N_{\mathrm{S}}}\{I_i^{\mathrm{Diff}}(j)\}^2}{N_{\mathrm{S}}}. \tag{10}$$

The minimum of mse can be an indicator to two similar transmission data sets while the minimum of the standard deviation as given by Eq. (7) indicates that elements of $I_i^{\mathrm{Diff}}(j)$ differ too little from the mean value. This again implies that the two transmission data sets, which produced that particular $I_i^{\mathrm{Diff}}(j)$ array, have too much similarity. The 0° and 360° will have the highest probability for the lowest sigma.

For tomographic reconstruction reported in this paper, the index $N_{\mathrm{P}}^{\#}$ found on the basis of minimum σ was used for further processing the data. It is also to be noted that slight mismatch in the rotary speed of the mechanism and the data acquisition speed may not produce visible artefact of the kind described above in case of circularly symmetric objects as all projections would be characteristically the same. Fig. 3 shows a schematic diagram of the operations carried out for this purpose.

4. Results and discussion

In order to experimentally validate the proposed correction method as described above, a test specimen (A) was designed to highlight the

artefacts in the reconstructed tomographic images. Fig. 4 shows a diagrammatic cross-section of the specimen. As evident, the detector array does not have very fine resolution and the experiment was carried out to verify the proposed correction method. The test specimen contained objects of dimension comparable to the detector resolution and of high contrast from the background. This was to ensure that the artefact due to the problem discussed above and the effect of corrections applied are visualized properly.

Three aluminium plates (1 mm thick) are concentrically placed and held by two circular perspex plates. Out of these, two Al plates are at 90° from each other while the third one makes an angle of 135° from both of them. The phantom does not have a 120° separation between the plates as it may show extra minima in sigma at 120° and 240° location. Table 2 shows all the parameters of the different scanning sequences. The experimentally acquired 1600 angular projections (N_P) were used to find out the value of $N_P^{\#}$. The resulting angular projections were resampled by a factor of four to get N_P^{+} equally spaced projections so that N_S and N_P^{+} are commensurate with each other. All the pre-processing were carried out on the I_t measurements as described above and afterwards, $P_\phi(t)$ values were calculated for tomographic image reconstruction. As an example, Fig. 5 shows a graphical plot of $\sigma(I_i^{Diff}(t))$ for $1 \leqslant i \leqslant 1600$. The first dip marked with the left arrow corresponds to 0° projection while the dip marked with the right arrow corresponds to approximately 360° angular position. This graph corresponds to the scan code (d) in Table 2. The acquired transmission data

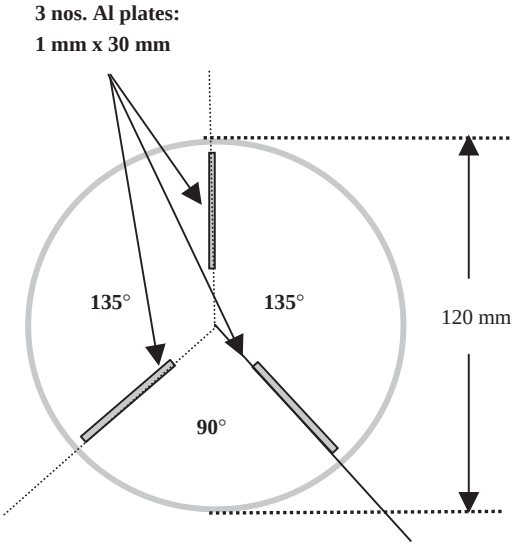

Fig. 4. A typical cross-section of the test specimen A.

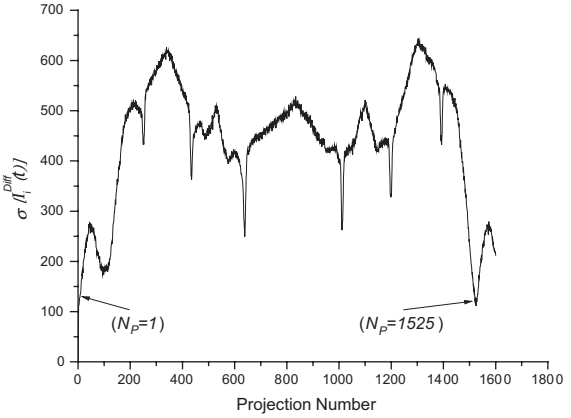

Fig. 5. Graphical plot of $\sigma(I_i^{Diff}(t))$ for projections $i = 1-1600$ for scan code d in Table 2 for the test specimen (Fig. 4).

Table 2
Scanning and correction parameters for test specimen (X-ray tube voltage: 100 kV_P, tube current: 0.7 mA)

Scan. code	N_S	Programmed angular speed (°/s)	Programmed N_p	$\sigma_{min}(N_P^{\#})$	$mse_{min}(N_P^{\#})$	Resampled index N_P^{+}	$\Delta\phi$ (deg)	CT image matrix (pixels)
a	260	27.6	1600	100.50(1571)	10,335(1571)	392	0.917	260^2
b	260	27.9	1600	106.60(1565)	11,827(1565)	391	0.920	260^2
c	260	28.2	1600	113.14(1543)	13,110(1543)	385	0.933	260^2
d	260	28.6	1600	111.61(1525)	12,483(1525)	381	0.944	260^2
e	260	28.9	1600	108.53(1510)	12,088(1510)	377	0.954	260^2
f	260	29.2	1600	101.98(1488)	10,440(1488)	372	0.968	260^2

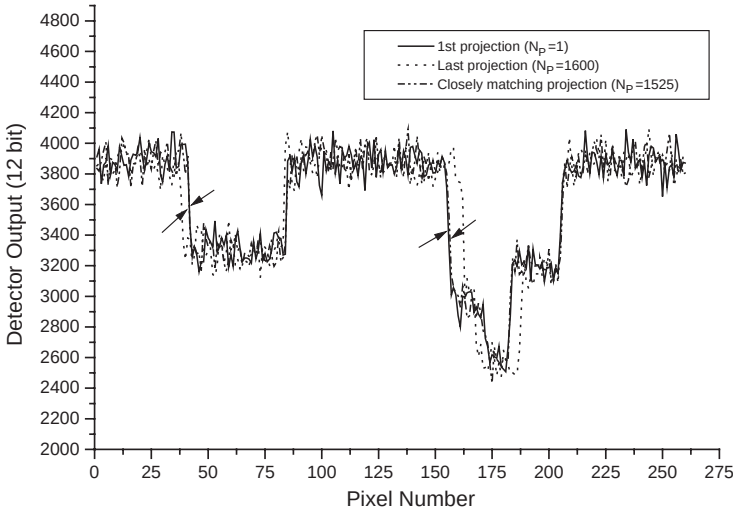

Fig. 6. A plot of transmission data profiles for projection numbers 1, 1525 and 1600 showing degree of matching achieved.

profiles for the projection numbers 1, 1525 and 1600 are shown graphically on the same scale in Fig. 6. The arrows on the graph highlight the degree of matching achieved between the data profiles numbered 1 and 1525. These transmission profiles are for the phantom shown in Fig. 4. Fig. 7 shows a plot of $N_P^{\#}$ corresponding to the σ_{min} values for different angular speeds of the specimen platform. As expected, $N_P^{\#}(\sigma_{min})$ decreases monotonically with decreasing angular speed.

Fig. 8 shows the reconstructed cross-section of the test specimen (Fig. 4) without applying the proposed correction. As per Fig. 4, three distinct lines are expected in the CT image. It is expected that the multiple images are due to the lack of synchronization in the angular speed of the scanning mechanism and the data acquisition system. The transmission data pertaining to this scan was then processed and Fig. 9 shows the CT image of the same plane through the specimen. Scan code (f) in Table 2 lists the scanning and reconstruction parameters. Though only one set of CT images (Figs. 8 and 9) of the test specimen is shown here for comparison, reconstructions carried out for scan codes (a−e) in Table 2 validates the numerical approach for minimization of the resulting artefact. It can be inferred that in case of an object having perfect circular symmetry, all the projections may be statistically similar. It would be

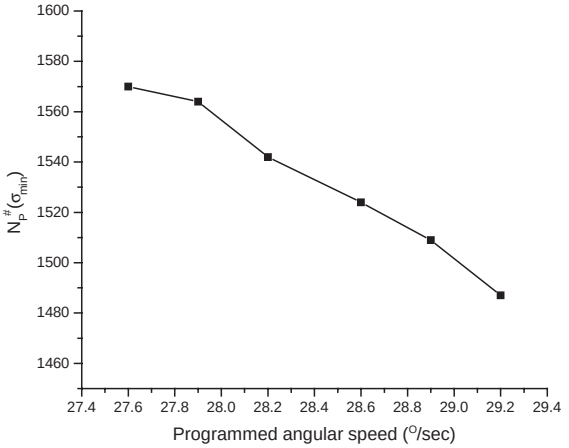

Fig. 7. Graphical plot of $N_P^{\#}(\sigma_{min})$ versus angular speed (°/s) of the rotary mechanism (Table 2) for the test specimen (Fig. 4).

interesting to examine a cylindrical object having very little circular asymmetry. For this purpose, another specimen (B) was fabricated from a solid block (OD = 50 mm) of cast acrylic material (perspex). Two holes (dia. 2 and 3 mm) were drilled at different radial distances from the centre. These holes introduced a little circular asymmetry in the cylindrical object. This specimen was scanned at three slightly different angular speeds causing deliberately introduced synchronization mismatch between the LDA data acquisition

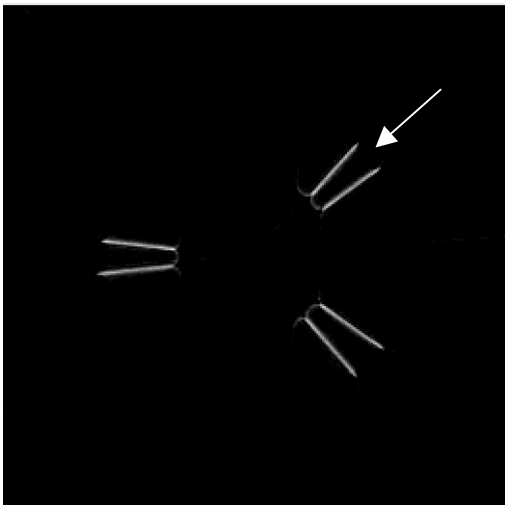

Fig. 8. Reconstruction of the cross-section (Fig. 4) before applying correction.

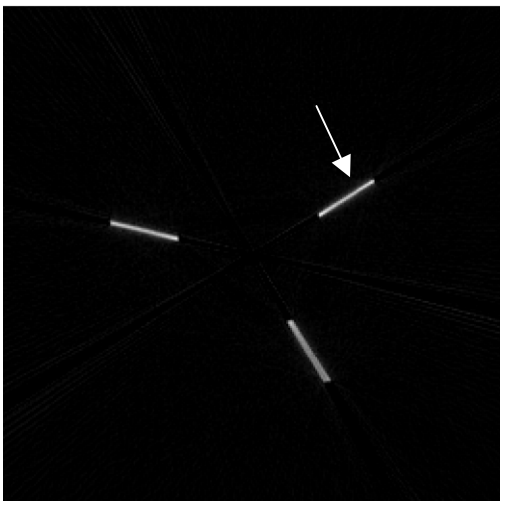

Fig. 9. Reconstruction of the cross-section (Fig. 4) after applying correction.

system and the scanning mechanism. A clear degradation in the quality of the reconstructed CT images was observed when the acquired data sets were not corrected. The sigma curve for perspex phantom is shown in Fig. 10. It does have a minima (marked with right arrow) in addition to the one corresponding to 0° angular location. It is not very much perceivable visually. This is obvious as the object has very little asymmetry. The

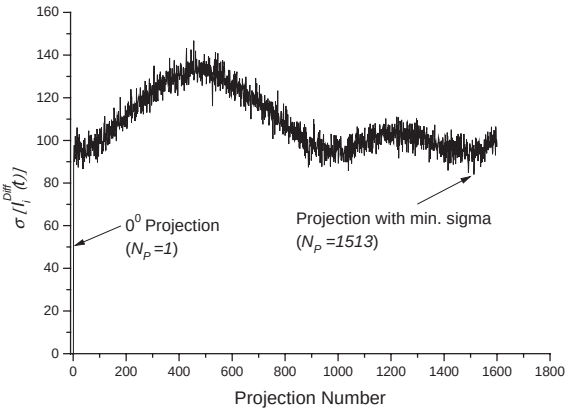

Fig. 10. Graphical plot of $\sigma(I_i^{\mathrm{Diff}}(t))$ for projections $i = 1-1600$ for the perspex phantom.

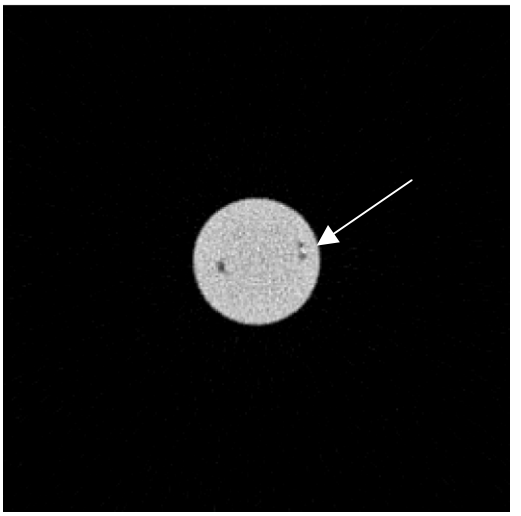

Fig. 11. CT image of the test specimen B before applying correction.

software routine looks at the sigma data corresponding to each index (N_{P}) for finding the minima. For example, Fig. 11 shows the reconstructed CT image without the suggested correction and Fig. 12 is the CT image of the same cross-section after the correction was applied. These figures refer to an angular scanning speed of 29.2°/s. Finally, a low-density composite material block (specimen C) with some debonded layers was scanned at two different angular speeds and tomographic images were generated for a typical

plane. Table 3 lists all the relevant parameters for these scans. Figs. 13 and 15 show the CT images without corrections being applied to the transmission data. The same data sets were then used after applying the suggested correction to reconstruct CT images as shown in Figs. 14 and 16. The marked clarity seen in these test scans suggests that the correction procedure is effective in a variety of specimens.

A limiting factor with the proposed correction method is that, because the projections are discretely sampled, a measured projection may not exist corresponding to the view angle 360°. Also, depending upon the coarseness of the angular sampling and the explicit geometry of the attenuating object, the estimated value of $\Delta\phi$ may have some error. In addition, it is assumed that the angular speed of the rotating system is fairly constant. The rotating mechanism is driven by a dedicated stepper motor controller and drive unit. The speed of the rotating mechanism depends upon the programmed pulse rate, which is generated by the onboard controller. Standard stepper motor controllers are quite stable and accurate upto 16 k pps. Finally, we can have a few words on the choice of σ and mse (Eqs. (7) and (10)). In fact, both these two parameters provided the same index to the near 360° projection. This can be seen from the columns of $\sigma_{\min}(N_P^{\#})$ and $\mathrm{mse}_{\min}(N_P^{\#})$ data in Tables 2 and 3. Any one can be used as far as the work reported in the paper is concerned.

5. Conclusion

It is observed that a lack of synchronization between mechanical scanning mechanism and data

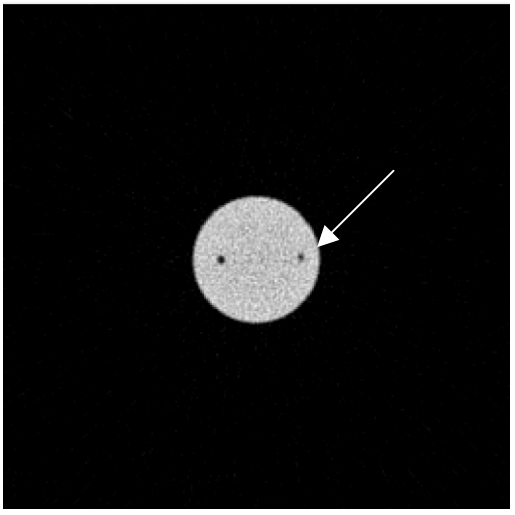

Fig. 12. CT image of the test specimen B after applying correction.

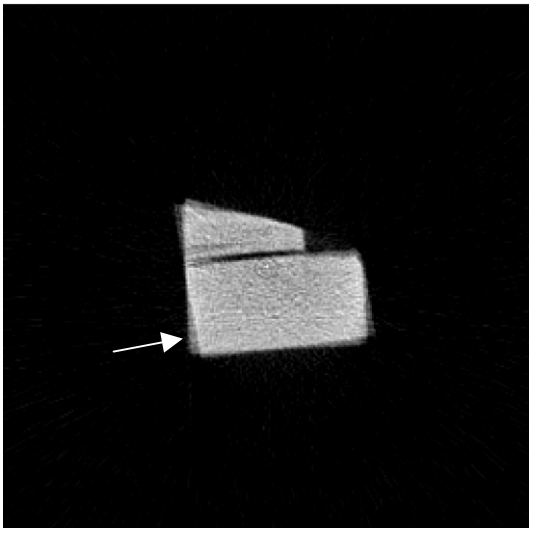

Fig. 13. CT image of the specimen C (scan code a, Table 3) before applying correction.

Table 3
Scanning parameters for composite sample (X-ray tube voltage: 100 kV_P, tube current: 0.7 mA)

Scan. code	N_S	Programmed angular speed (°/s)	Programmed N_p	$\sigma_{\min}(N_P^{\#})$	$\mathrm{mse}_{\min}(N_P^{\#})$	Resampled index N_P^{+}	$\Delta\phi$ (deg)	CT image matrix (pixels)
a	260	27.9	1600	89.86(1558)	8087(1558)	389	0.925	260^2
b	260	28.6	1600	87.96(1513)	7836(1513)	378	0.952	260^2

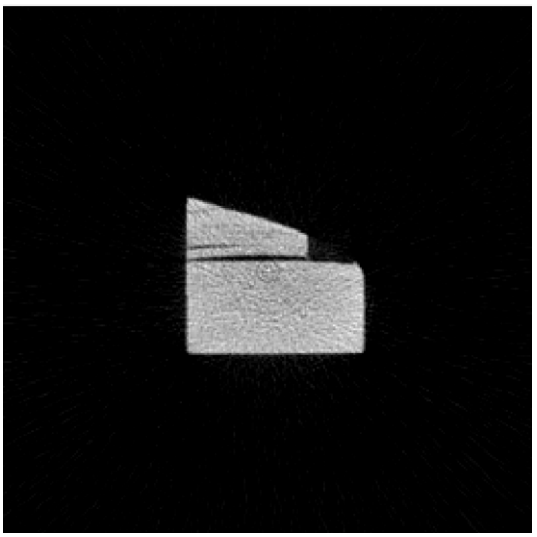

Fig. 14. Reconstruction of the specimen C cross-section after applying correction.

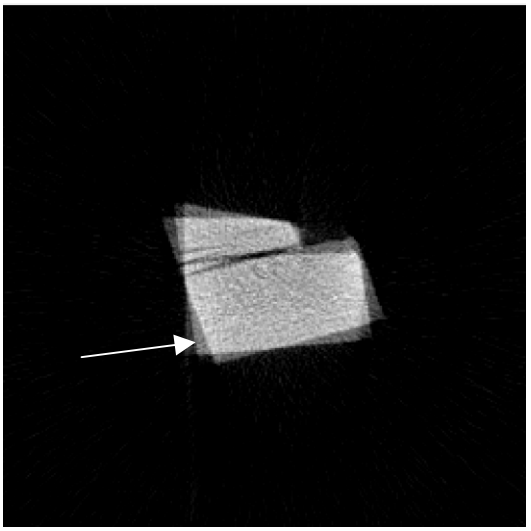

Fig. 15. CT image of the specimen C (scan code b, Table 3) before applying correction.

acquisition of a computed tomography imaging system results in artefacts in reconstructed CT images. A method for correcting transmission data matrix based on the principle of finding out minimum of difference signal has been discussed.

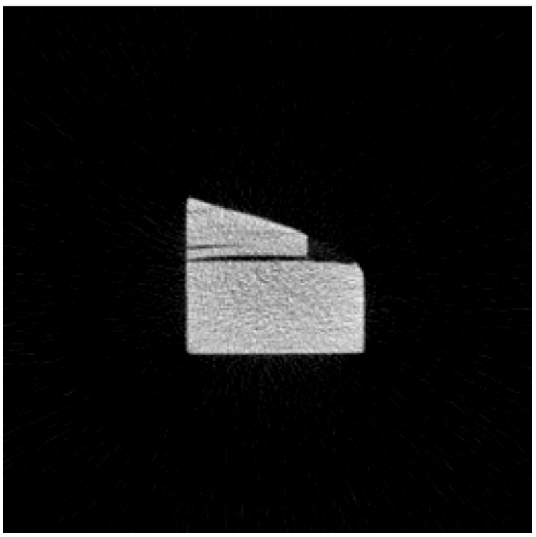

Fig. 16. Reconstruction of the specimen C cross-section after applying correction.

The set of multiple one-dimensional transmission data profiles at different angular positions are used in the correction algorithm to find out near -360° projection in a continuous rotate-only industrial CT scanning geometry. The first one-dimensional profile recorded is treated as the 0° position data and remaining profiles are then subtracted from this one. Experimental results were obtained which validate the algorithm adopted. The basic idea proposed is to identify the projection that most closely resembles 0° projection and designate it as 360° projection. This method may be particularly useful where experimental tomographic imaging systems are designed around self-contained subsystems and where hardware interfacing may be difficult to achieve. The algorithm suggested in the experiment may well be incorporated in the preprocessing software prior to tomographic image reconstruction. Possible limitations and drawbacks of the suggested method have also been discussed.

Acknowledgements

Authors are thankful to the Head of Isotope Applications Division, BARC for his constant

support. Thanks are also due to all the technical staff of the engineering workshop of Isotope Applications Division.

References

[1] C.R. Crawford, G.T. Gulberg, Med. Phys. 15 (1) (1988) 67.
[2] R. Waggener, M. Lee, D. Mickish, J. Lange, J. Feldmeier, Med. Phys. 16 (2) (1989) 197.
[3] R. Gordon, IEEE Trans. Nucl. Sci. NS-21 (1974) 78.
[4] D. Mishra, K. Murlidhar, P. Munshi, Numer. Heat Transfer Part B 35 (1999) 485.
[5] F. Natterer, The Mathematics of Computerized Tomography. Wiley & B G Teubner, New York, Stuttgart, 1986, p. 138.
[6] A.C. Kak, M. Slaney, Principles of Computerized Tomographic Imaging, IEEE Press, USA, 1988.
[7] G.T. Herman (Ed.), Image Reconstructions from Projections, Implementation and Applications. Topics in Applied Physics, Spring, Berlin, 1979, p. 32.
[8] F. Natterer, J. Siam, Appl. Math. 53 (2) (1993) 358.
[9] D.L. Parker, Med. Phys. 9 (2) (1982) 254.
[10] M.D. Silver, Med. Phys. 27 (4) (2000) 773.
[11] M.D. Seshadri, D.W. Miller, D. Campbell, J.M. Hill, Appl. Radiat. Isot. 41 (1990) 963.
[12] D.A. Fry, C.R. Pearsall, A.C. Guu, Appl. Radiat. Isot. 41 (1990) 1131.
[13] ASTM 2000 Designation: E1441-00 Annual Book of ASTM Standards USA (ASTM), p. 11.
[14] User manual of Xscan08, Rev. C 2000 Detection Technology Inc., Finland.
[15] U. Kumar, G.S. Ramakrishna, A.S. Pendharkar, G. Singh, Nucl. Instr. and Meth. A 490 (2002) 379.